Philosophical Magazine,
Vol. ??, No. ?, Month?-? 2005, 1–21

Taylor & Francis
Taylor & Francis Group

Stress field and interaction forces of dislocations in anisotropic multilayer thin films

XUELI HAN and NASR M. GHONIEM*

Department of Mechanical and Aerospace Engineering, University of California, Los Angeles, Los Angeles, CA 90095-1597, USA

(*Received 17 January 2004; in final form 22 October 2004*)

Utilizing Fourier transforms, the elastic field of three-dimensional dislocation loops in anisotropic multilayer materials is developed. Green's functions and their derivatives, obtained first in the Fourier domain and then in the real domain by numerical inversion, are used in integrals to determine the elastic field of dislocation loops. The interaction forces between dislocations and free surfaces or interfaces in multilayer thin films are then investigated. The developed method is based on rigorous elasticity solutions for dislocations approaching to within one to two atomic planes from the interface. For a dislocation in one layer, the interface *image force* is determined mainly by the elastic moduli and thicknesses of neighbouring layers. When a dislocation approaches an interface between two layers, within 10–20 atomic planes, the image force changes rapidly. Interaction forces are then kept constant up to the interface. The model shows that, when a dislocation crosses an interface from a soft to a hard layer, additional external forces must be applied to overcome an elastic mismatch barrier. The developed method extends the concept of the *Kohler barrier* in 2D, and shows that the interface force barrier not only depends on the relative ratio of the elastic moduli of neighbouring layers, but also on the 3D shape of the dislocation, the number of interacting adjacent layers, and on layer thicknesses.

Keywords: Anisotropic multilayer thin films; Dislocation loops; Interaction forces

1. Introduction

The physics of strength in confined small volumes requires development of accurate methods for the determination of dislocation interaction mechanisms. In particular, the influence of confining surfaces on dislocation motion, configuration, and force distribution as dislocations approach or cross interfaces needs precise quantification. Many recent technology applications are based on thin films or coatings that are composed of alternating layers of different materials. Other important systems where the dislocation–interface interaction plays a significant role can be found in sandwiched interphases, nano-layered materials, quantum dots on substrates and fine precipitate dispersions in alloys. For these systems, free surfaces and interfaces

*Corresponding author. Email: ghoniem@ucla.edu

Philosophical Magazine
ISSN 1478–6435 print/ISSN 1478–6443 online © 2005 Taylor & Francis Ltd
http://www.tandf.co.uk/journals
DOI: 10.1080/14786430412331331907

have important effects on the stress field of dislocations and hence on plastic deformation at the nano- and micro-scales. In nano-scale and micro-scale applications, the ratio of interface to volume becomes very large compared with bulk applications, and hence interfacial effects are expected to become dominant. Yield and post-yield properties of multi-layer nano-scale materials deviate from the properties of bulk materials, and cannot be explained by conventional plasticity theory. New mechanisms and relationships between the mechanical properties and interfacial properties (including structure) in nano-scale multilayer materials need to be explored with accurate theoretical methods.

The strength of multilayer materials is derived from the resistance of interfaces between layers to dislocation motion, as dislocations cross them from one layer to another. To design ultra-strong, yet ductile materials, one needs to understand how dislocations interact with interfaces. Resistance forces to dislocation motion can result from structural effects and/or elastic moduli mismatches. The influence of interface structure is attributed to several sources: lattice constant mismatch that generates coherency strains, misfit interfacial dislocations in semi-coherent and incoherent interfaces, stacking fault energy mismatch of the incoming and outgoing slip planes, slip system mismatch that forces cross-slip of dislocations across the interface, and dislocation core spreading into the interface [1–3]. Elastic moduli mismatch (discontinuity across the interface) induces dislocation image forces, which appear to be the dominant source of resistance [1–3]. We will therefore focus our attention here on dislocation image forces in multilayer materials.

The computational framework of Dislocation Dynamics (DD) has been developed for fundamental descriptions of plasticity and fracture. The approach relies on direct numerical simulations of the collective motion of dislocation ensembles without *ad hoc* assumptions, e.g. [4–7]. However, most DD applications so far are for the deformation of bulk, isotropic materials. Very little attention has been paid to finding solutions for the elastic field of three-dimensional dislocations near interfaces, and no exact analytical solutions exist even for the simple case of a straight dislocation segment in two half-space materials. Using approximate methods or numerical calculations, a few recent studies have attempted to treat the influence of free surfaces (i.e. *image effects*) on the dynamics of dislocation systems. These are summarized as

(i) In the superposition method, combined with the finite element or boundary element methods, numerical techniques are utilized to satisfy traction equilibrium at free surfaces [8, 9].
(ii) In the surface dislocation method, surface dislocation loop distributions are invoked so as to approximately satisfy interfacial or free surface traction conditions at specific surface collocation points [10].
(iii) Approximate methods are based on Lothe's solution [5, 11], or assume rigid interfaces [12].
(iv) Elasticity methods for the solution of a dislocation segment near a free surface [13, 14], or the Boussinesq solution for a point force on a free surface [15].
(v) The Phase Field approach, where use is made of a regular grid to efficiently compute the Fourier functions [16].
(vi) An extension of the method developed by Devincre, Kubin and co-workers, where Green's functions need not be defined [17].

The approaches described above have their limitations. Numerical methods (the finite element (FEM) or the boundary element (BEM)) suffer from the necessity to re-calculate the superposed FEM or BEM solution every time step. As dislocations approach the surface or interface, the mesh must be refined, and the solution is not convergent if special care is not exercised with dislocation singularities. Other methods are limited to the simplest free surface boundary condition, and their extensions to anisotropic multilayered materials are not readily attainable without *ad hoc* approximations. The numerous interfaces in multilayer thin films pose particular difficulties for all existing methods. No precise solutions for 3D arbitrary shape dislocations in anisotropic multilayer materials are thus available.

The objective of the present work is to develop rigorous and precise solutions for the elastic field of dislocation loops of arbitrary shape in anisotropic multilayer thin films, and to investigate interfacial image forces on dislocations. Methods for determination of the stress field and interface/free surface interaction forces will be considered for a number of cases currently of practical interest:

(i) A single thin film layer on a substrate. Here, we consider variations of hard/soft films on a substrate.
(ii) A capped thin film on a substrate, with variations of the thickness of the capped layer.
(iii) A dislocation loop crossing an interface between two adjacent layers.

The selected examples are intended to show features of the stress field and interaction forces of dislocations in anisotropic, multilayer thin films.

We will first utilize the method of Yang and Pan [18, 19] to calculate Green's functions and their derivatives in anisotropic multilayers in section 2. The elastic field of dislocations in multilayer thin films is then presented in section 3, with numerical applications for infinitesimal and finite dislocation loops. Analysis of the effects of image forces due to free surfaces and interfaces will be presented for static dislocation loops in section 4, where we consider dislocations in a film-on-substrate, capped film-on-substrate, and a dislocation crossing an interface. We finally present our conclusions in section 5.

2. Green's tensor functions and their derivatives

Elastic Green's functions, which describe the displacement response of a linear elastic solid to a point force, are fundamental ingredients in many methods developed for understanding the mechanics of materials. A description of the internal or *self* stress field of materials containing defects is critically dependent on accurate knowledge of elastic Green's functions. Interaction forces between defects and the elastic energy stored around them can be obtained once Green's functions are determined. More recently, Molecular Dynamics (MD) computer simulations of defect interactions have utilized Green's functions to connect atomistic simulation regions to the elastic continuum, e.g. [20]. Computer simulations of defect interactions by Kinetic Monte Carlo (KMC), e.g. [21], or by DD, require Green's functions as essential elements. Unfortunately, however, analytical solutions of Green's functions are not available, with the exception of a few cases. Moreover, numerical methods for 3D Green's functions in finite spaces of general elastic anisotropy are also very limited [22].

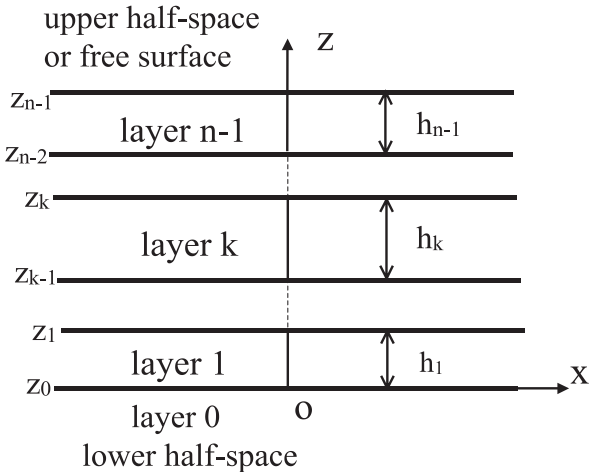

Figure 1. Geometry of a multilayered thin film system.

Using 2D Fourier transforms, numerical solutions for anisotropic Green's functions in half-space and bimaterials have recently been obtained [23]. Pan and coworkers developed Green's functions in anisotropic layered structures, such as bimaterials [24], trimaterials [19], and multilayers [18, 25]. In this section, we briefly present the basic procedure to calculate Green's functions in anisotropic multilayered materials using the 2D Fourier transform combined with the generalized Stroh's formalism. The presentation in this section follows [18, 19, 22–24]. Subsequent developments for the elastic field and dislocation–interface interaction forces in the following sections will utilize the methods of these references, and hence a concise outline of the method for the determination of Green's tensor functions will be given.

Consider a stack of N layers, each of uniform thickness, perfectly bonded at their interfaces, as shown in figure 1. Variables describing the geometry and coordinates are also shown in the figure. We assume here that each layer is homogeneous, anisotropic and with distinct elastic properties.

The Green's tensor function $G_{ij}(\mathbf{x}, \mathbf{x}')$ is the displacement component in the x_i direction at point $\mathbf{x}$ in response to a unit body force in the x_j direction, applied at point $\mathbf{x}'$. These functions satisfy the equilibrium equation

$$C_{ijkl}(\mathbf{x})G_{km,lj}(\mathbf{x}, \mathbf{x}') = -\delta_{im}\delta(\mathbf{x}, \mathbf{x}'). \tag{1}$$

Now, introduce the 2D Fourier transform, applied to the in-plane coordinates (x_1, x_2), for any function $f(x_1, x_2, x_3)$ in the real domain. The corresponding function in the Fourier domain, $\tilde{f}(\xi_1, \xi_2, x_3)$, is given by

$$\tilde{f}(\xi_1, \xi_2, x_3) = \int_{-\infty}^{\infty}\int_{-\infty}^{\infty} f(x_1, x_2, x_3)\, e^{\mathbf{i}(\xi_1 x_1 + \xi_2 x_2)}\, \mathrm{d}x_1\, \mathrm{d}x_2. \tag{2}$$

Transforming equation (1), we obtain

$$C_{i\alpha k\beta}\xi_\alpha\xi_\beta\tilde{G}_{km} + \mathbf{i}(C_{i\alpha k3} + C_{i3k\alpha})\xi_\alpha\tilde{G}_{km,3} - C_{i3k3}\tilde{G}_{km,33} = e^{\mathbf{i}\xi_\alpha x'_\alpha}\delta_{im}\delta(x_3, x'_3), \tag{3}$$

where $\alpha, \beta = 1, 2$.

The system of ordinary differential equations (3) is second order, with the independent variable being the out-of-plane coordinate x_3. The general solution for this system, which gives Green's functions in the Fourier domain, is

$$\tilde{\mathbf{G}}(\xi_1, \xi_2, x_3; \mathbf{x}') = e^{\mathbf{i}\xi_\alpha x'_\alpha}[\tilde{\mathbf{G}}^\infty(\xi_1, \xi_2, x_3; x'_3) + \mathbf{i}\eta^{-1}(\bar{\mathbf{A}}\langle e^{-\mathbf{i}\bar{\mathbf{p}}\eta x_3}\rangle \mathbf{V} + \mathbf{A}\langle e^{-\mathbf{i}\mathbf{p}\eta x_3}\rangle \mathbf{W})], \tag{4}$$

where (η, θ) are the polar coordinates of (ξ_1, ξ_2), $\mathbf{V}$ and $\mathbf{W}$ are unknown constant matrices to be determined from boundary conditions, $\langle e^{-\mathbf{i}\mathbf{p}\eta x_3}\rangle = \mathrm{diag}[e^{-\mathbf{i}p_1\eta x_3}, e^{-\mathbf{i}p_2\eta x_3}, e^{-\mathbf{i}p_3\eta x_3}]$, p_i $(\mathrm{Im}(p_i) > 0)$ and $\mathbf{A} = (\mathbf{a}_1, \mathbf{a}_2, \mathbf{a}_3)$ being the eigenvalues and eigenmatrix of

$$[\mathbf{Q} + p_i(\mathbf{R} + \mathbf{R}^{\mathrm{T}}) + p_i^2\mathbf{T}]\mathbf{a}_i = 0, \tag{5}$$

$$Q_{ik} = C_{ijks}n_j n_s, \quad R_{ik} = C_{ijk3}n_j, \quad T_{ik} = C_{i3k3},$$

with $n_1 = \cos\theta$ and $n_2 = \sin\theta$.

In the solution given by equation (4), Green's functions (displacements) are separated into two parts: a singular full-space solution $\tilde{\mathbf{G}}^\infty$ (with elastic properties being those where the field point $\mathbf{x}$ is located, and the point force is applied at $\mathbf{x}' = (0, 0, x'_3)$), and a regular complementary part. Details of the separated solution, and the numerical procedure for matching boundary conditions in the Fourier domain and subsequent inversion to the real domain are given in appendix A.

3. Stress field of dislocation loops

3.1. *General procedure*

Once Green's tensor functions are determined, the elastic field of a dislocation loop can be constructed by numerical integration. The displacement vector field of a dislocation loop can be expressed as [26]

$$u_i(\mathbf{x}) = -\int_S C_{jlmn}(\mathbf{x}')b_m \frac{\partial}{\partial x'_l} G_{ji}(\mathbf{x}', \mathbf{x})n_n(\mathbf{x}')\,\mathrm{d}S(\mathbf{x}'), \tag{6}$$

where $G_{ji}(\mathbf{x}', \mathbf{x})$ are the Green's functions at $\mathbf{x}'$ due to a point force applied at $\mathbf{x}$, S is any arbitrary surface capping the loop, n_n is a unit normal to S and b_m is the Burgers vector. Equation (6) can be rewritten in another convenient form as

$$u_i(\mathbf{x}) = -\int_S \sigma_{mni}(\mathbf{x}', \mathbf{x})b_m n_n(\mathbf{x}')\,\mathrm{d}S(\mathbf{x}'), \tag{7}$$

where $\sigma_{mni}(\mathbf{x}', \mathbf{x})$ is the mnth Green's stress component at a field point $\mathbf{x}'$ due to a unit point force in the i direction applied at the source point $\mathbf{x}$.

The stress field produced by the dislocation loop can be expressed as

$$\sigma_{ij}(\mathbf{x}) = -C_{ijkl}(\mathbf{x})\int_S C_{pqmn}(\mathbf{x}')b_m \frac{\partial^2}{\partial x_l \partial x'_q} G_{pk}(\mathbf{x}', \mathbf{x})n_n(\mathbf{x}')\,\mathrm{d}S(\mathbf{x}'), \tag{8}$$

or

$$\sigma_{ij}(\mathbf{x}) = -C_{ijkl}(\mathbf{x})\int_S \frac{\partial}{\partial x_l}\sigma_{mnk}(\mathbf{x}', \mathbf{x})b_m n_n(\mathbf{x}')\,\mathrm{d}S(\mathbf{x}'). \tag{9}$$

When the dimensions of the dislocation loop are much smaller than the distance between any source point on the loop and the field point, the loop can be considered as infinitesimal, and its field can be obtained directly from equations (6)–(9) without the surface integration:

$$\sigma_{ij}(\mathbf{x}) = -C_{ijkl}(\mathbf{x})\frac{\partial}{\partial x_l}\sigma_{mnk}(\mathbf{x}', \mathbf{x})b_m n_n(\mathbf{x}')\,\delta A, \tag{10}$$

where δA is the loop area.

The derivatives of Green's functions with respect to both field and source points are needed. First, we consider derivatives with respect to a source point. From expressions (A4) and (A5), the derivatives with respect to x_1' and x_2' in the Fourier domain are obtained as

$$\partial\tilde{\mathbf{G}}_k/\partial x_\alpha' = \mathbf{i}\xi_\alpha\tilde{\mathbf{G}}_k, \quad \alpha = 1, 2, \tag{11}$$

where $\tilde{\mathbf{G}}_k$ denotes Green's functions or Green's stresses of the kth layer in the Fourier domain. The derivatives of Green's functions with respect to x_3' can be expressed as

$$\begin{aligned}&\partial\tilde{\mathbf{G}}_k/\partial x_3' \\ &\quad = e^{\mathbf{i}\xi_\alpha x_\alpha'}\left[\frac{\partial\tilde{\mathbf{G}}_k^\infty}{\partial x_3'} + i\eta^{-1}\left(\bar{\mathbf{A}}_k\langle e^{-\mathbf{i}\bar{\mathbf{p}}_k\eta(x_3 - z_{k-1})}\rangle\frac{\partial\mathbf{V}_k}{\partial x_3'} + \mathbf{A}_k\langle e^{-\mathbf{i}\mathbf{p}_k\eta(x_3 - z_k)}\rangle\frac{\partial\mathbf{W}_k}{\partial x_3'}\right)\right].\end{aligned} \tag{12}$$

Similarly, one can obtain the derivatives of Green's stresses. When we calculate Green's functions, $\mathbf{V}_k$ and $\mathbf{W}_k$ can be determined. However, their derivatives $\partial\mathbf{V}_k/\partial x_3'$ and $\partial\mathbf{W}_k/\partial x_3'$ are not available, and we need to calculate them separately for determination of the stress field. Performing derivatives on the boundary conditions, equations (A7) (and (A8) if the nth layer has a free surface), we obtain

$$\left(\mathbf{Z}_k(z_k) - \mathbf{Z}_{k+1}(z_k)\right)\begin{pmatrix}\partial\mathbf{V}_k/\partial x_3' \\ \partial\mathbf{W}_k/\partial x_3' \\ \partial\mathbf{V}_{k+1}/\partial x_3' \\ \partial\mathbf{W}_{k+1}/\partial x_3'\end{pmatrix} = \begin{pmatrix}\partial\tilde{\mathbf{u}}_{k+1}^\infty/\partial x_3' \\ \partial\tilde{\mathbf{t}}_{k+1}^\infty/\partial x_3'\end{pmatrix}(z_k) - \begin{pmatrix}\partial\tilde{\mathbf{u}}_k^\infty/\partial x_3' \\ \partial\tilde{\mathbf{t}}_k^\infty/\partial x_3'\end{pmatrix}(z_k),$$

$$k = 0, \ldots, n-1, \tag{13}$$

$$\left(\bar{\mathbf{B}}_n\langle e^{-\mathbf{i}\mathbf{p}_n\eta h_n}\rangle\,\mathbf{B}_\mathbf{n}\right)\begin{pmatrix}\partial\mathbf{V}_n/\partial x_3' \\ \partial\mathbf{W}_n/\partial x_3'\end{pmatrix} = -\frac{\partial\tilde{\mathbf{t}}_n^\infty(z_n)}{\partial x_3'}. \tag{14}$$

Solving the linear algebraic equations (13) (and (14) when needed), $\partial\mathbf{V}_k/\partial x_3'$ and $\partial\mathbf{W}_k/\partial x_3'$ $(k = 0, \ldots, n)$ can be determined. Because the coefficient matrices of equations (13), (14) and (A7), (A8) are the same, the inverse matrix need to be calculated only once. Taking the inverse Fourier transforms of equations (11) and (12), the derivatives with respect to $\mathbf{x}'$ are finally obtained.

3.2. *Method validation*

Before presenting numerical examples for dislocations, we validate the numerical accuracy of the present method. First, the Green's functions are carried out to

Table 1. Green's functions and stresses in a transversely isotropic half-space.

	Present	[24]
G_{ij}		
(11) = (22)	0.64233731	0.64233732
(33)	0.39504885	0.39504886
σ_{ijk}		
(131) = (232)	−1.34601662	−1.34601664
(113) = (223)	0.65825907	0.65825908
(333)	−11.9102534	−11.9102536

Table 2. Stress components of an infinitesimal dislocation loop in infinite medium.

	Present	Analytical [28]
σ_{11}	$2.1848151419 \times 10^{-2}$	$2.1848151417 \times 10^{-2}$
σ_{12}	$-1.3500288206 \times 10^{-2}$	$-1.3500288215 \times 10^{-2}$
σ_{13}	$-3.1747583852 \times 10^{-2}$	$-3.1747583875 \times 10^{-2}$
σ_{22}	$4.3579468058 \times 10^{-3}$	$4.3579467801 \times 10^{-3}$
σ_{23}	$9.5804728556 \times 10^{-3}$	$9.5804728141 \times 10^{-3}$
σ_{33}	$-7.0685196040 \times 10^{-3}$	$-7.0685195763 \times 10^{-3}$

compare the present results with existing solutions. It is found that we predict the same results as those obtained by Pan and Yuan [24] for anisotropic half/bi-half space, and Pan [27] for isotropic/transverse isotropic multilayers to relative accuracies of less than 10^{-6}. Table 1 shows Green's functions and stresses in a half-space ($x_3 \leq 0$) compared with known results by Pan and Yuan [24]. In this example, the material is transversely isotropic with $E_1 = E_2 = 1$, $E_3 = 10$, $G_{13} = 1$, $\nu_{12} = \nu_{31} = 0.3$. The source and field points are located at $(0, 0, -1)$ and $(0, 0, -0.75)$, respectively.

After validating the accuracy of Green's functions, the fields of an infinitesimal dislocation in infinite space are calculated and compared with the analytical results of Kroupa [28], see table 2. In this example, the material constants are: $E = 1$, $\nu = 0.3$, the dislocation is located at $(0, 0, 0)$ with the Burgers vector $\mathbf{b} = [100]$ and has a surface area δA on the plane (001), and the field point is at $(1, -0.5, 0.1)$. In the table, the stress is normalized to the volume $|\mathbf{b}|\delta A$. It can be seen that the results agree to a relative error of less than 10^{-9}. The same relative accuracy was also found when the present method is compared with the results for a circular dislocation loop in an infinite anisotropic medium [29].

3.3. *Infinitesimal dislocation loop in film-on-substrate*

Here, we show results for a small (infinitesimal) dislocation loop in a thin film on top of a very thick substrate, which is approximated as half-space. The film–substrate system is shown in figure 2, with a thin film (of thickness h) on top of a half-space substrate. The substrate material ($z < 0$) is copper, and the thin film is either aluminium or nickel. The materials selected for this example are all fcc cubic anisotropic crystals, with their crystallographic axes [100], [010] and [001] taken to coincide with the x, y and z directions, respectively. The elastic constants are taken from [30]. The anisotropic ratio $A = 0.5(C_{11} - C_{12})/C_{44}$ is 3.21, 1.21 and 2.52 for Cu, Al and Ni, respectively ($A = 1$ for isotropic materials).

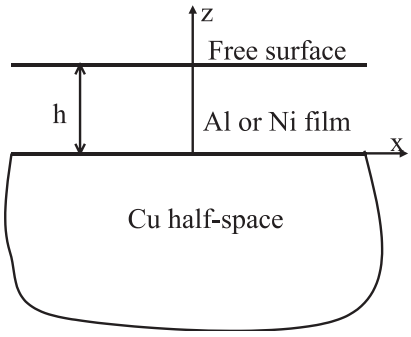

Figure 2. Geometry and coordinate system for the film-on-substrate arrangement.

Assuming an infinitesimal dislocation is located at the middle of the thin film (i.e. $\mathbf{x}' = (0, 0, 0.5h)$), with its surface area δA lying on the (111) plane, and $\mathbf{b}$ along the $[\bar{1}10]$ direction. Figures 3 and 4 show contour lines for the out-of-plane stress σ_{32} and the in-plane stress σ_{12} on the plane $y = 0$, respectively. The stresses are normalized to $|\mathbf{b}|\delta A h^{-3} \times 10^{10}$. From these figures, it can be seen that the out-of-plane stresses are forced to decrease identically to zero at the surface to satisfy free traction boundary conditions. On the other hand, in-plane stresses are released at the free surface. At the interface ($z = 0$), the out-of-plane stress components are continuous, while in-plane components experience jumps as a result of the discontinuity in the elastic properties. As one approaches the interface from a softer material to a harder one (e.g. Al to Cu), the stress fields, especially in-plane components, are arrested. Once one moves across the interface, in-plane components are released, and experience a jump. It is also observed that the stress fields are usually more complex for a source in a material with a high anisotropic ratio (e.g. Ni), while they show smoother variations in nearly isotropic materials (e.g. Al).

3.4. *Dislocation loop in film-on-substrate*

To understand the effects of free surfaces and the interfaces on stress distributions around finite-size dislocation loops, we present here results for a circular loop. As an example, we choose the same (Al) film and (Cu) substrate, as shown in figure 2. The circular shear loop (radius, $R = 0.5h$) is located in the middle of the film $(0, 0, 0.5h)$, and lies on the (111) plane, with $\mathbf{b}$ along the $[\bar{1}10]$ direction. Figure 5(a) shows the $\sigma_{23} = 0.15$ iso-surface (normalized to $|\mathbf{b}|R^{-1} \times 10^{10}$). For comparison purposes, the same iso-surface in an Al infinite space is shown in figure 5(b). To satisfy the zero traction boundary condition at the top surface, the out-of-plane stress iso-surface is totally confined below it. The volume of the same iso-surface expands into the softer material across the interface. This means that the range of influence of a dislocation loop in a harder layer expands into neighbouring softer layers, as compared with the infinite medium case.

4. Dislocation–interface interaction

So far, we have determined the main characteristics of the elastic stress field induced by finite-size or infinitesimal dislocations in a multilayer material. However, an area

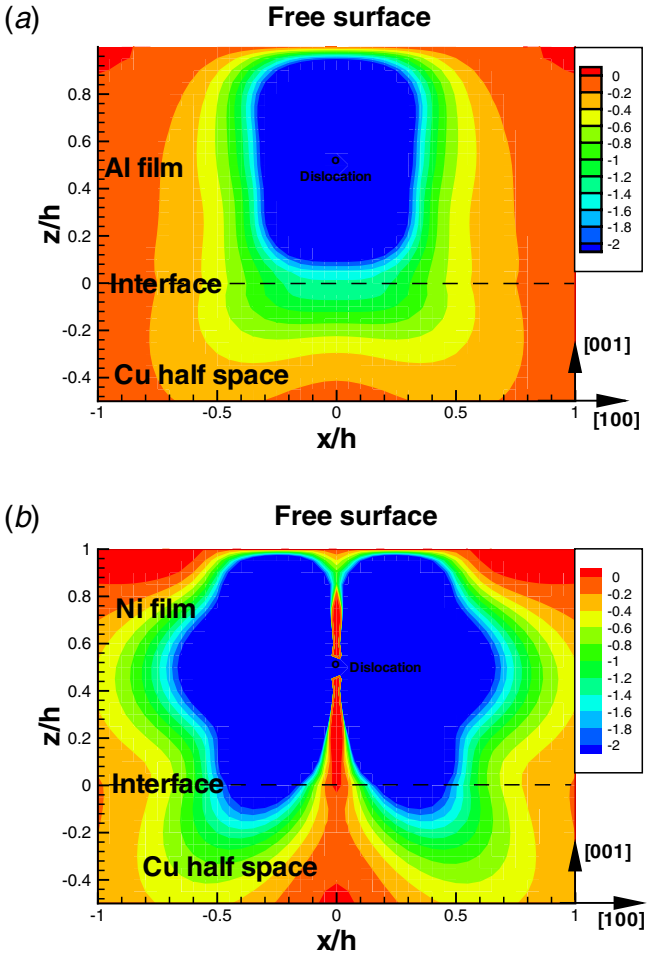

Figure 3. σ_{32} stress contours on the $y=0$ plane due to an infinitesimal dislocation loop at $(0, 0, 0.5h)$ in (*a*) Al (film) on a Cu (substrate) and (*b*) Ni (film) on a Cu (substrate).

of great interest, especially in relationship to DD simulations, is the distribution of configurational forces on dislocations as they move or change their shapes. A dislocation will experience a configurational force (so-called Peach–Koehler force) if it attempts motion or change in shape in a stress field, $\boldsymbol{\sigma}$. The force, $\mathbf{f}$, on a dislocation loop segment, $d\mathbf{l}$, of a 3D loop of a burgers vector $\mathbf{b}$ can be determined by the Peach–Koehler formula:

$$\mathbf{f} = \boldsymbol{\sigma} \cdot \mathbf{b} \times d\mathbf{l}. \tag{15}$$

We will divide the stress field induced by a dislocation into two parts: the full-space solution $\boldsymbol{\sigma}^{\infty}$ and the image contribution $\boldsymbol{\sigma}^{\mathrm{I}}$. This separation will allow us to consider interface effects on dislocation forces, and to calculate the dislocation self-force without ambiguities. For a dislocation loop which is located totally within a single material layer, the stress separation is clear. $\boldsymbol{\sigma}^{\infty}$ corresponds to the stress field induced by the dislocation in a homogeneous, infinite medium with a material that is identical to the layer where the dislocation is located. The stress field $\boldsymbol{\sigma}^{\infty}$

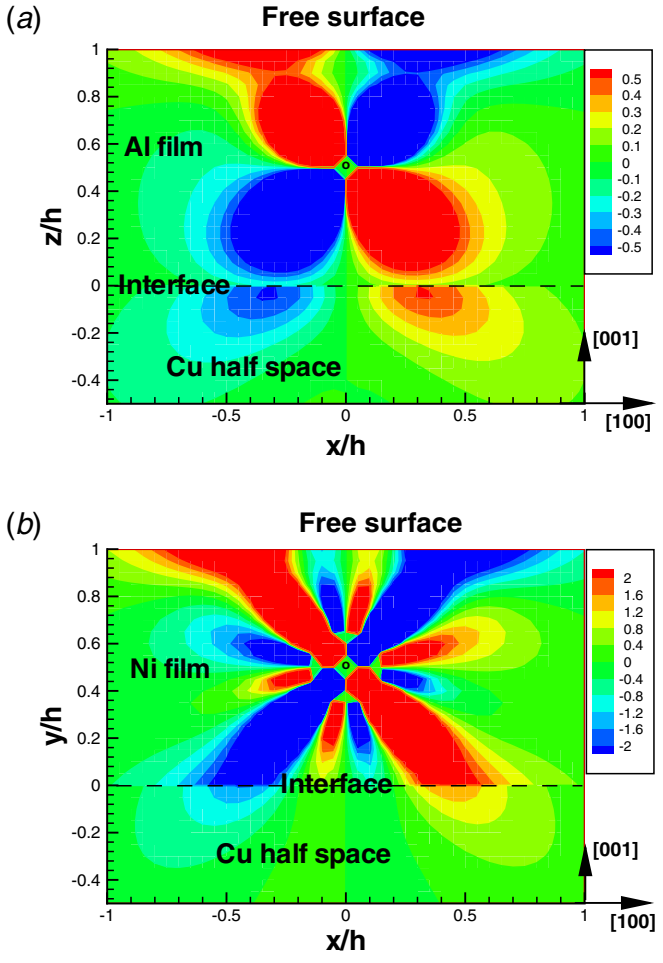

Figure 4. σ_{12} stress contours on the $y=0$ plane due to an infinitesimal dislocation loop at $(0, 0, 0.5h)$ in (*a*) Al (film) on a Cu (substrate) and (*b*) Ni (film) on a Cu (substrate).

of a dislocation in an infinite anisotropic material can be expressed as a line integral along the dislocation loop by the formula of Mura [26]. $\boldsymbol{\sigma}^{\infty}$ will then induce a *self-force* on the dislocation, which can be obtained by the procedure of Gavazza and Barnett [31]; for details, see the work of Han *et al*. [29]. The force induced by the regular part of the stress field, $\boldsymbol{\sigma}^{\mathrm{I}}$, is usually called the *image force*, and can be calculated directly by applying the Peach–Koehler formula.

When a dislocation loop does not reside totally in one single layer, but crosses one or more interfaces and material layers, the separation of self-force from the image force is not so straightforward. In this case, we distinguish between them in the following way. Consider a point **P** on the loop, and assume that the whole loop is in a homogeneous, infinite medium, with a material identical to that in which the point **P** is located. This loop will induce a stress field $\boldsymbol{\sigma}^{\infty}$ and self-force on the unit dislocation segment where **P** is located. Now, subtract $\boldsymbol{\sigma}^{\infty}$ from the total stress field to obtain the image stress $\boldsymbol{\sigma}^{\mathrm{I}}$, which is regular. We use this part of the stress field to calculate, unambiguously, the image force on the dislocation segment at **P**.

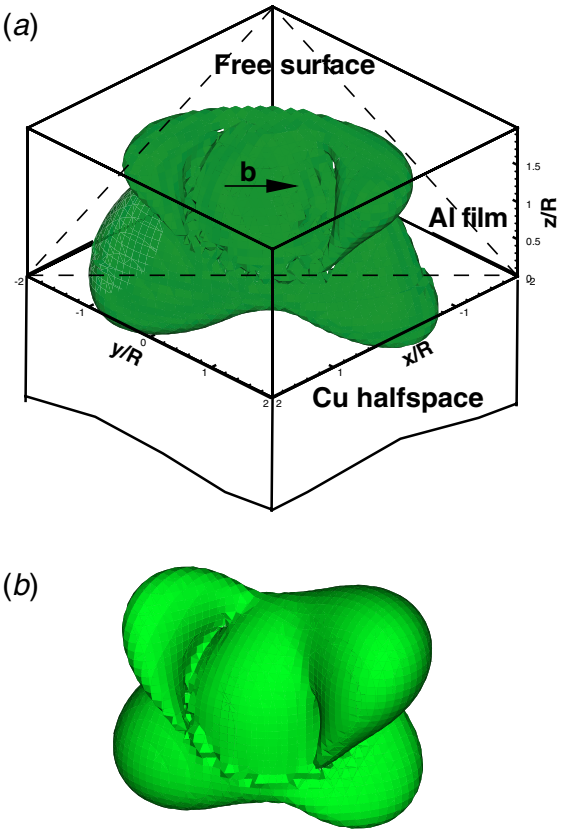

Figure 5. σ_{23} stress iso-surface for a circular shear dislocation loop in (*a*) Al (film) on a Cu (substrate) and (*b*) Al infinite space.

In the following, we focus our attention on image forces on dislocations in a variety of representative surface/interface conditions.

4.1. *Film-on-substrate*

Anisotropic thin films on extended substrates are common in many nano-scale and micro-scale applications. The distribution of image forces on dislocations in such systems determines how dislocations approach free surfaces or the interface between the film and substrate. We consider here the same film-on-substrate system with a representative circular dislocation loop as in the previous section. The distribution of image forces on a circular dislocation loop in an Al and Ni film on top of an extended Cu substrate is shown in figures 6(*a*) and (*b*), respectively. The force is per unit length, and is normalized to $|\mathbf{b}|^2 R^{-1} \times 10^{10}$. The free surface tends to attract the entire dislocation line. However, the closer a dislocation segment is to the free surface, and the harder the material is, the larger the surface image force. When a dislocation segment approaches an interface from a softer material to a harder one (Al to Cu), the interface tends to block it, while from a harder material to a softer side, the dislocation is attracted to the interface. It is noted from the figures that the image force is truly three dimensional, and that the

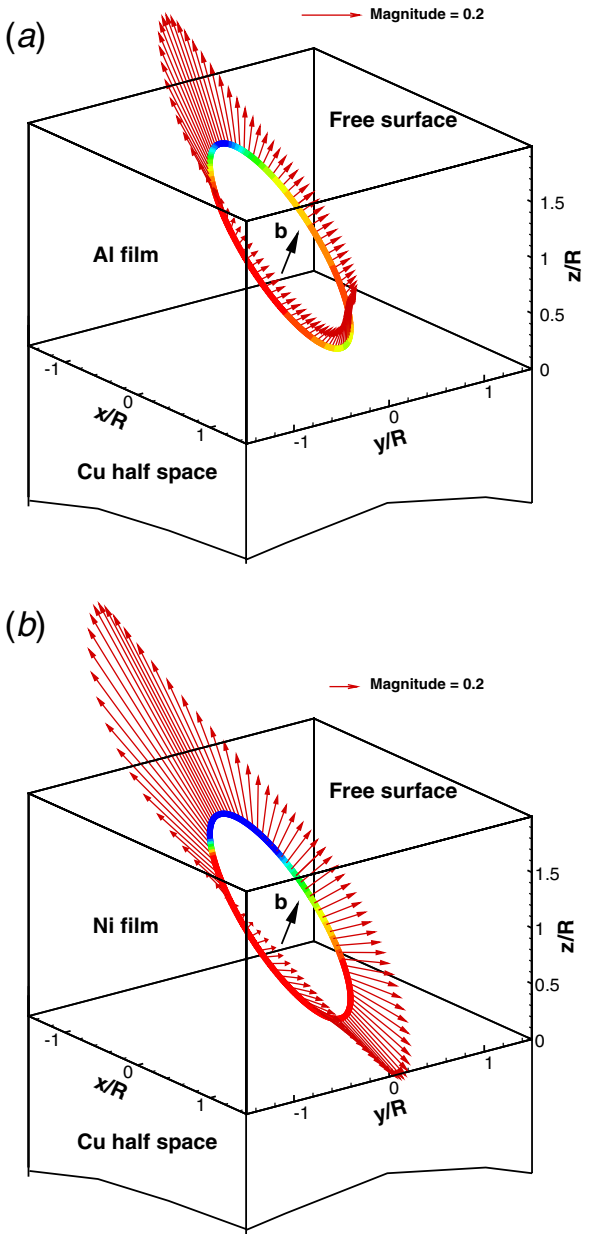

Figure 6. Free surface and interface image force distributions on a circular dislocation loop in (*a*) Al (film) on a Cu (substrate) and (*b*) Ni (film) on a Cu (substrate).

distribution, magnitude and direction cannot be easily obtained from simple image constructions based only on 2D analysis. This complexity presents significant computational challenges to the development of DD models that faithfully account for surface and interface effects. The other observation here is that while glide is the dominant component of surface and interface image forces, there are considerable contributions from climb as well.

4.2. *Capped film-on-substrate*

A capping layer is often deposited on top of thin films for environmental protection, or to engender additional and desirable physico-chemical properties. Also, if the thin film is oxidizable, and is used at ambient conditions, a naturally grown oxide capping layer will be present. We consider here the influence of capping layers on the behaviour of dislocations confined within thin films. Strong interaction between the dislocation and a free surface or an interface results in its deformation, such that a large section of a dislocation loop is straight and parallel to the free surface or interface. We examine here interaction forces between dislocation loops and multiple interfaces and a free surface. We use a proto-typical dislocation loop to examine these interaction forces. We choose an Al film (width h) on a Cu substrate. However, the film here is capped with another thin Cu film, of width h_c. An oblong dislocation loop is located in the middle of the Al thin film. The oblong loop is composed of two straight segments parallel to the interfaces, and are connected by two half-circular segments, as shown in figure 7. The length of the straight part, and the width of the oblong section of the loop, respectively, are L and D, with $L=2D$ and $D=h$. The distribution of image forces on the loop is shown in figures 7(a) and (b) for various thicknesses of the capping layer. Image forces are normalized to $|\mathbf{b}|^2h^{-1}\times 10^{10}$.

Numerical results show that image forces on the straight section of the loop near the capping layer display a strong dependence on the layer thickness. Image forces vary rapidly with increasing capping layer thickness for $h_c<h$. However, the magnitude and direction of forces tend to those for $h_c\to\infty$. These conclusions mean that, for thin capping layers (e.g. $h_c<h$), other nearby interfaces (e.g. the free surface of the capping layer) have strong coupling effects on force distributions of the dislocation. Thus, and in this case, the stress field and image force distributions are controlled by interacting nearby interfaces. For thicker capping layers, however, one may be able to use image forces resulting from an infinitely extended half-plane. We also consider image force variation as the dislocation approaches the Al–Cu interface. When a dislocation segment is very close to an interface, and distances to other interfaces are comparatively far, the image force exerted on this dislocation segment is dominated by the closest interface.

4.3. *Dislocation loop across an interface*

One of the most critical considerations in designing ultra-strong materials is the ability to confine dislocations in very thin layers, without allowing them to penetrate across interfaces. The strength of a nano-layered system is greatly enhanced if interfaces can indeed offer the necessary resistance to their motion, even if high levels of stresses are applied. The maximum difference between the image force on a dislocation segment in one material and the corresponding force after the dislocation segment has crossed the interface into a neighbouring material is known as the *Koehler barrier* [32]. The applied stress must be large enough to overcome this barrier, in addition to other configurational resistance forces arising from structural effects of the interface itself. As such effects are outside the scope of the present investigation, and require atomistic simulations, we address here the behaviour of dislocation segments in as much as the Kohler barrier is concerned. It is to be noted here that the origin of this barrier is the change in the stiffness of the interatomic potential (e.g. the curvature of the pair part of the potential)

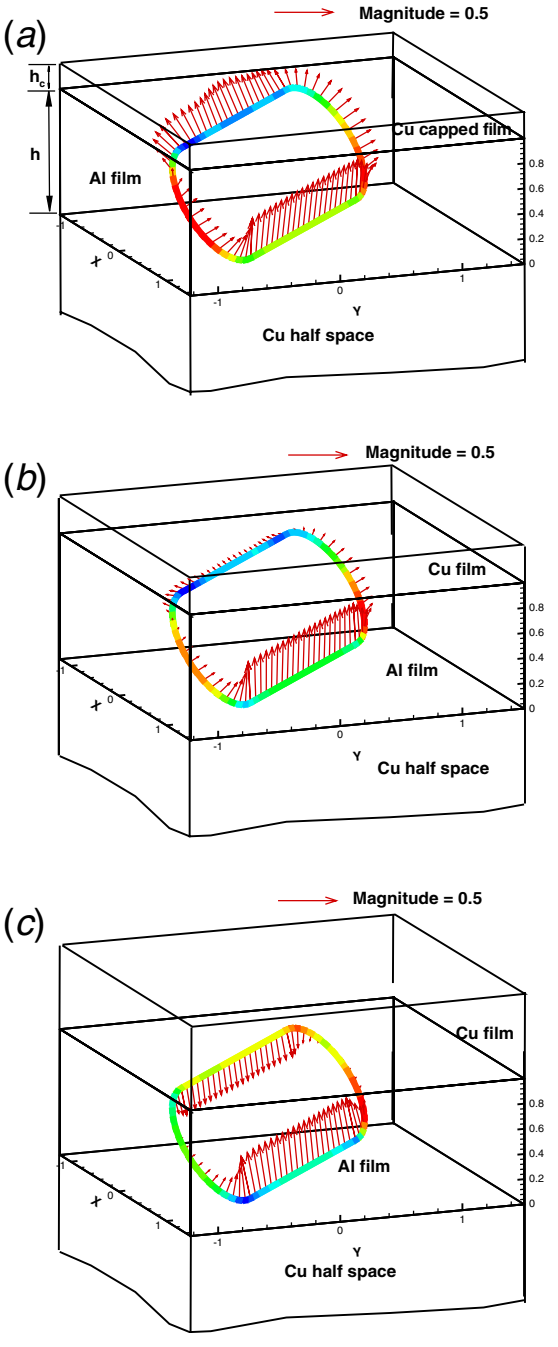

Figure 7. Image force of an oblong dislocation loop in an Al film on a Cu substrate. The Al film is capped by a Cu layer of thickness $h_c = 0.1h$ (*a*), $0.2h$ (*b*) and $0.5h$ (*c*).

as dislocations cross from one material to another. In other words, sudden changes in the elastic constants across an interface are reflected in a jump in the magnitude of the image force on a dislocation segment. Since infinitesimal linear elasticity is used here, we would not expect the results to be rigorously accurate very near

the interface, and some approximation is required. The original concept of Koehler was based on saturating (i.e. truncating) the image force as the dislocation comes within a specified minimum distance of a dislocation core width of $2|\mathbf{b}|$ [32]. We follow here the same model to deduce the resistance of an interface to dislocations crossing it. Image forces will be calculated with the methods outlined earlier, and assumed to be valid up to a cut-off distance of one to two atomic layers from the interface. This assumption is also consistent with evaluations of self-forces using infinitesimal linear elasticity [7].

To examine the nature of the Koehler barrier, we choose here the case of a circular dislocation loop approaching an interface across two half-spaces. Figures 8(*a*)–(*c*) show the force distributions, including the self-force and the image force on the loop, as the loop is brought to closer proximity from the interface, and then finally crosses the interface. In this example, the loop is on the (111) plane with $\mathbf{b}$ along $[\bar{1}10]$ and a radius $R = 200|\mathbf{b}|$. The Al–Cu interface is along the [001] direction. The image force is very large only on the part of the loop that is close to the interface. The force is relatively small everywhere else, and decreases rapidly with distance away from the interface, as can be observed in figures 8(*a*)–(*c*).

Force variations, for the two points A and B (which are the closest points when the corresponding loop segment approaches the interface), are displayed in figures 9(*a*) and (*b*), respectively. Forces are plotted as functions of the distance of the point from the interface, and they include self- and image contributions. They are also separated into glide and climb components. The 2D image force approximation (*Koehler barrier*), estimated for an infinite straight dislocation near the interface, is calculated and shown in the figures as dashed lines [32]. It can be seen that when the loop is in one material (not across the interface), only the glide component of the image force at the leading point (nearest to the interface) is close to the Koehler estimate. The climb component and other loop configurations show drastic differences from the Koehler estimate as a result of the three dimensionality of the problem.

The direction of the in-plane curvature of the loop is chosen as the positive direction for the self- and glide forces, while the positive direction of the climb force is defined along the plane normal to (111). It is observed that when the distance between the leading point on the dislocation and the interface is less than $20|\mathbf{b}|$, image forces increase sharply and interface effects become dominant. If linear elasticity is taken as strictly valid, the force is singular at the interface. Here, however, we assume its validity up to a minimum approach distance on the order of the dislocation core width of $2|\mathbf{b}|$. The results displayed in figures 9(*a*) and (*b*) show the complexity of loop force variations in the close proximity of the interface. First, the jump in the self-force is a result of the sudden change in the elastic constants of the medium, and the magnitude of the force scales with the stiffness of the material. What is interesting to note here is that while the climb component of the image force (including the Koehler barrier) is dominant on the closest segment when the loop crosses from the softer (Al) to the harder (Cu) material, as seen in figure 9(*a*), the situation is reversed when the loop crosses from Cu into Al (see figure 9(*b*)). This unique asymmetry is a result of the fact that the entire loop geometry determines the split between the climb ($\mathbf{f}_c$) and glide ($\mathbf{f}_g$) components of the force. Such detailed behaviour can be critical to whether the dislocation segment would prefer to climb and cross-slip across an interface, or just simply continue gliding on the same glide plane if the orientation is favourable.

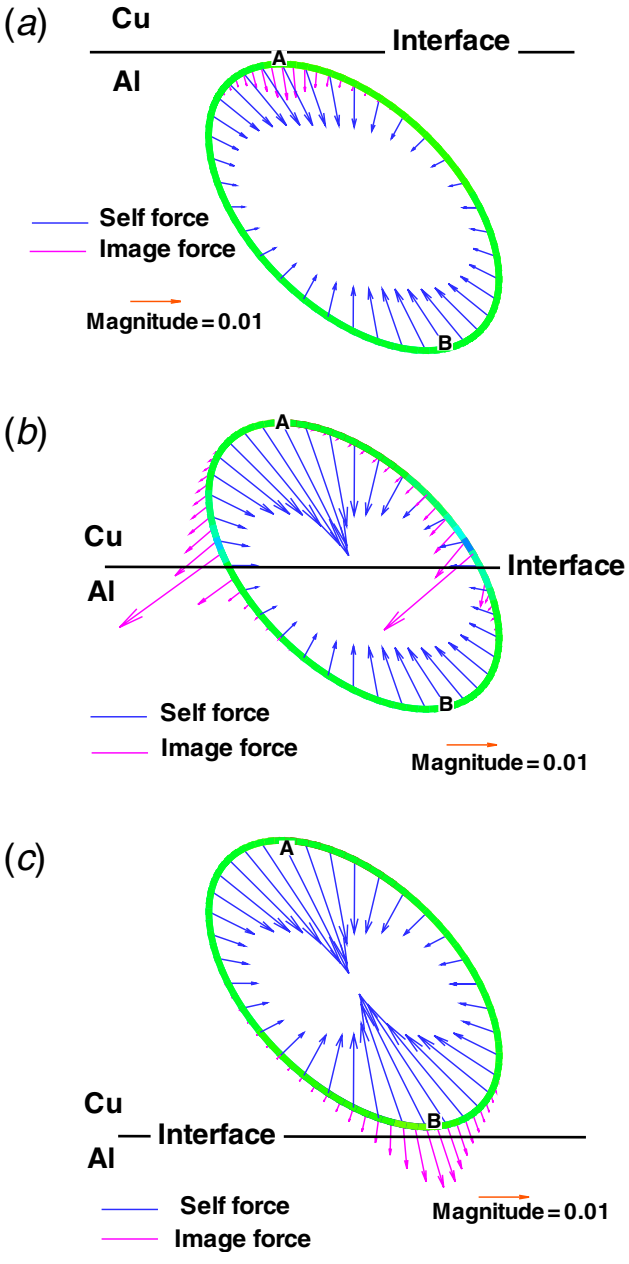

Figure 8. Force distributions on a dislocation loop: (*a*) as it approaches the interface, but is contained in a softer material of small elastic anisotropy; (*b*) as it straddles the interface; and (*c*) the loop is totally contained in a harder material of large elastic anisotropy.

5. Summary and conclusions

The interest in the mechanical behaviour of ultra-strong materials, prepared by sputter deposition of multiple nano-layers, and in the reliability and failure of thin films in microelectronic and other applications, demands thorough understanding

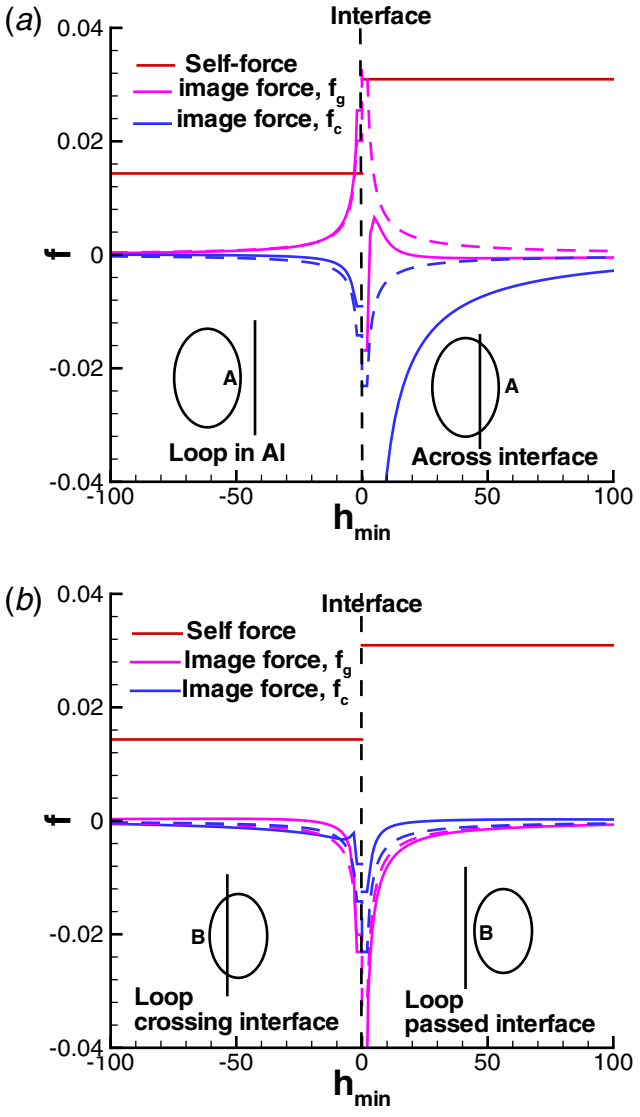

Figure 9. Dependence of force components on (*a*) the leading point A and (*b*) the trailing point B, as functions of their distance from the interface. Koehler's 2D solution is represented by dashed lines.

of dislocation behaviour in such material systems. In these applications, interfaces play a prominent role in controlling dislocation motion and, hence, the strength and deformability. The present investigation provides a computational method by which one can assess forces and interactions amongst dislocations in anisotropic multi-layer materials. Future developments of DD, including applications in these systems, rely on understanding accuracy limits of approximate numerical methods. For example, the limits of existing methods for incorporation of free surface effects in DD simulations (e.g. FEM, BEM, surface dislocations, etc.) may be determined by detailed comparisons with the present method. We have shown here that the

elastic field and configurational forces of dislocation loops of arbitrary geometry and in any type of anisotropic layered thin film can be rigorously determined if the thickness of the film is much less than its in-plane dimensions. Starting from the point force problem of Green's functions in a multi-layer thin film, the elastic field of dislocation loops is obtained by a surface integral. The key issue here is that 2D Fourier transforms can be used, together with the generalized Stroh's formalism, to obtain the solution, first in Fourier space, and then in real space by numerical inversion. To expedite the computational aspects of these steps, the approach recently proposed by Yang and Pan [19] is adopted.

Elastic field calculations of dislocations in anisotropic multilayer materials can be performed with great accuracy, without any limits on the number of material layers, or dislocation shapes. However, direct implementation of this procedure in DD simulations may still be limited to systems containing few dislocations at present as a result of the heavy computational cost, despite efforts to expedite calculations of Fourier inversion integrals. Approximate methods to develop line rather than surface integrals will benefit from the present investigation, since numerical errors due to approximations can be readily determined.

Through a systematic numerical study of stress fields and forces induced by dislocations in multi-layered materials, we draw the following conclusions.

(i) Stress fields and image forces on dislocations are greatly influenced by the presence of interfaces. Thus, interface image forces cannot be ignored or simply approximated without careful considerations. Generally, however, the nearest interface to a dislocation segment determines the majority of image effects. However, in layered systems where layer thicknesses are small (e.g. nano-layered materials), several neighbouring interfaces (approximately two to four) participate simultaneously.

(ii) If applied forces on dislocations are large, the influence of interfaces on dislocation motion may be only significant very close to the interface, within less than 10 nm. In such cases, the closest interface becomes the most dominant.

(iii) When a dislocation segment is near an interface, the image force usually drives the segment towards a softer material and away from a harder one. Thus, when we consider events occurring near an interface, such as dislocation threading, or dislocation nucleation from interfaces, the force induced by the interface becomes very large and local. As an approximation, one may consider the effect from this interface only, and ignore interaction effects from other interfaces.

(iv) Stress fields emanating from dislocations are confined or released by a neighbouring harder layer or softer layer, respectively.

(v) Interfacial image forces are inherently three dimensional, since they cannot be simply determined by geometric image constructions, as is customary in some DD simulations. Both glide and climb components must be considered in the analysis of near-interface processes, such as nucleation and threading. The barrier to climb may be smaller than that for glide, and hence screw components may prefer to cross-slip rather than glide across an interface. Only the glide component of the image force at the leading point (nearest to the interface) is close to the 2D Koehler estimate, when the loop is totally within one layer. The climb component and other loop configurations show drastic differences from the Koehler estimate.

(vi) Dislocation segments crossing interfaces display irreversibility of motion. When a dislocation crosses from a softer to a harder material, it may prefer to climb. If the same segment attempts to return from the harder to the softer material, however, its glide Koehler barrier is smaller, and will hence glide across rather than retrace its previous path. This mechanism cannot be explained by 2D approximations, since it is a result of the asymmetry created across the interface by the presence of the dislocation loop itself in two different media.

Acknowledgements

We acknowledge the support of the U.S. National Science Foundation (NSF) for this research through grant No. DMR-0113555, and the support of the U.S. Air Force Office for Scientific Research (AFOSR) through grant No. F49620-03-1-0031 with UCLA.

Appendix A: Numerical evaluation of Green's tensor functions

In the Fourier domain, we have

$$\tilde{\mathbf{G}}^{\infty}(\xi_1,\xi_2,x_3;x_3') = \mathbf{i}\eta^{-1}\begin{cases} \mathbf{A}\langle e^{-\mathbf{i}\mathbf{p}\eta(x_3-x_3')}\rangle\mathbf{A}^{\mathrm{T}}, & x_3 < x_3', \\ -\bar{\mathbf{A}}\langle e^{-\mathbf{i}\bar{\mathbf{p}}\eta(x_3-x_3')}\rangle\bar{\mathbf{A}}^{\mathrm{T}}, & x_3 > x_3'. \end{cases} \tag{A1}$$

Green's stress tensor is defined as $\sigma_{jki} = C_{jklm}u_{li,m}$. Thus, the out-of-plane traction vector is $\mathbf{t} = (\sigma_{31i}, \sigma_{32i}, \sigma_{33i})$, and the in-plane stress vector is $\mathbf{s} = (\sigma_{11i}, \sigma_{12i}, \sigma_{22i})$. These can be expressed as

$$\begin{aligned}\tilde{\mathbf{t}}(\xi_1,\xi_2,x_3;\mathbf{x}') = e^{\mathbf{i}\xi_\alpha x_\alpha'}[&\tilde{\mathbf{t}}^{\infty}(\xi_1,\xi_2,x_3;x_3') \\ &+ (\bar{\mathbf{B}}\langle e^{-\mathbf{i}\bar{\mathbf{p}}\eta x_3}\rangle\mathbf{V} + \mathbf{B}\langle e^{-\mathbf{i}\mathbf{p}\eta x_3}\rangle\mathbf{W})],\end{aligned} \tag{A2}$$

$$\begin{aligned}\tilde{\mathbf{s}}(\xi_1,\xi_2,x_3;\mathbf{x}') = e^{\mathbf{i}\xi_\alpha x_\alpha'}[&\tilde{\mathbf{s}}^{\infty}(\xi_1,\xi_2,x_3;x_3') \\ &+ (\bar{\mathbf{C}}\langle e^{-\mathbf{i}\bar{\mathbf{p}}\eta x_3}\rangle\mathbf{V} + \mathbf{C}\langle e^{-\mathbf{i}\mathbf{p}\eta x_3}\rangle\mathbf{W})],\end{aligned} \tag{A3}$$

with

$$\tilde{\mathbf{t}}^{\infty}(\xi_1,\xi_2,x_3;x_3') = \begin{cases} \mathbf{B}\langle e^{-\mathbf{i}\mathbf{p}\eta(x_3-x_3')}\rangle\mathbf{A}^{\mathrm{T}}, & x_3 < x_3', \\ -\bar{\mathbf{B}}\langle e^{-\mathbf{i}\bar{\mathbf{p}}\eta(x_3-x_3')}\rangle\bar{\mathbf{A}}^{\mathrm{T}}, & x_3 > x_3', \end{cases}$$

$$\tilde{\mathbf{s}}^{\infty}(\xi_1,\xi_2,x_3;x_3') = \begin{cases} \mathbf{C}\langle e^{-\mathbf{i}\mathbf{p}\eta(x_3-x_3')}\rangle\mathbf{A}^{\mathrm{T}}, & x_3 < x_3', \\ -\bar{\mathbf{C}}\langle e^{-\mathbf{i}\bar{\mathbf{p}}\eta(x_3-x_3')}\rangle\bar{\mathbf{A}}^{\mathrm{T}}, & x_3 > x_3'. \end{cases}$$

The vectors $\mathbf{B}$ and $\mathbf{C}$ are related to $\mathbf{A}$ as

$$\mathbf{b}_i = (\mathbf{R}^{\mathrm{T}} + p_i\mathbf{T})\mathbf{a}_i, \qquad \mathbf{c}_i = \mathbf{D}_i\mathbf{a}_i,$$

with

$$D_{kli} = C_{1kl\alpha}n_\alpha + p_iC_{1kl3} \quad \text{for } k = 1,2, \text{ and } D_{3li} = C_{22l\alpha}n_\alpha + p_iC_{22l3}.$$

The general solutions (equations (4), (A2), and (A3)) have translational invariance with respect to x_3 (i.e. they remain valid if x_3 in $\langle e^{-\mathbf{i}\bar{\mathbf{p}}\eta x_3}\rangle$ and $\langle e^{-\mathbf{i}\mathbf{p}\eta x_3}\rangle$ is replaced with $(x_3-\gamma)$, with γ being an arbitrary real constant). Thus, Green's displacements and stresses for any layer k ($z_{k-1} < x_3 < z_k$) can be rewritten as

$$\begin{pmatrix}\tilde{\mathbf{G}}\\ \tilde{\mathbf{t}}\end{pmatrix}_k(x_3) = e^{\mathbf{i}\xi_\alpha x'_\alpha}\left[\begin{pmatrix}\tilde{\mathbf{G}}\\ \tilde{\mathbf{t}}\end{pmatrix}_k^{\infty}(x_3) + \mathbf{Z}_k(x_3)\begin{pmatrix}\mathbf{V}\\ \mathbf{W}\end{pmatrix}_k\right], \tag{A4}$$

$$\tilde{\mathbf{s}}_k(x_3) = e^{\mathbf{i}\xi_\alpha x'_\alpha}[\tilde{\mathbf{s}}_k^{\infty}(x_3) + (\bar{\mathbf{C}}_k\langle e^{-\mathbf{i}\bar{\mathbf{p}}_k\eta(x_3-z_{k-1})}\rangle\mathbf{V}_k + \mathbf{C}_k\langle e^{-\mathbf{i}\mathbf{p}_k\eta(x_3-z_k)}\rangle\mathbf{W}_k)], \tag{A5}$$

with

$$\mathbf{Z}_k(x_3) = \begin{pmatrix}\mathbf{i}\eta^{-1}\mathbf{A}_k & \mathbf{i}\eta^{-1}\mathbf{A}_k\\ \mathbf{B}_k & \mathbf{B}_k\end{pmatrix}\begin{pmatrix}\langle e^{-\mathbf{i}\bar{\mathbf{p}}_k\eta(x_3-z_{k-1})}\rangle & 0\\ 0 & \langle e^{-\mathbf{i}\mathbf{p}_k\eta(x_3-z_k)}\rangle\end{pmatrix}. \tag{A6}$$

If the 0th layer is a half-space, the finite solution requirement gives $\mathbf{V}_0 = \mathbf{0}$. Similarly, if the nth layer is a half-space, $\mathbf{W}_n = \mathbf{0}$.

The boundary conditions for perfectly bonded interfaces are expressed as

$$\left(\mathbf{Z}_k(z_k) - \mathbf{Z}_{k+1}(z_k)\right)\begin{pmatrix}\mathbf{V}_k\\ \mathbf{W}_k\\ \mathbf{V}_{k+1}\\ \mathbf{W}_{k+1}\end{pmatrix} = \begin{pmatrix}\tilde{\mathbf{G}}\\ \tilde{\mathbf{t}}\end{pmatrix}_{k+1}^{\infty}(z_k) - \begin{pmatrix}\tilde{\mathbf{G}}\\ \tilde{\mathbf{t}}\end{pmatrix}_k^{\infty}(z_k),$$
$$k = 0, \ldots, n-1. \tag{A7}$$

If the nth layer has a free surface along $x_3 = z_n$, we have

$$\left(\mathbf{B}_n\langle e^{-\mathbf{i}\mathbf{p}_n\eta h_n}\rangle\ \mathbf{B}_\mathbf{n}\right)\begin{pmatrix}\mathbf{V}_n\\ \mathbf{W}_n\end{pmatrix} = -\tilde{\mathbf{t}}_n^{\infty}(z_n). \tag{A8}$$

Equations (A7) and (A8) form a banded (with width 12) linear algebraic system of equations, which can be easily solved. After the unknowns $\mathbf{V}_k$ and $\mathbf{W}_k$ ($k = 0, \ldots, n$) are determined, the solutions for every layer in the Fourier domain are obtained. The corresponding physical-domain solutions are then recovered by the inverse Fourier transform:

$$f(x_1, x_2, x_3) = \frac{1}{(2\pi)^2}\int_0^{\infty}\int_0^{2\pi}\eta\tilde{f}(\eta, \theta, x_3)\, e^{-\mathbf{i}\eta(x_1\cos\theta + x_2\sin\theta)}\,\mathrm{d}\theta\,\mathrm{d}\eta. \tag{A9}$$

When applying the inverse transform to Green's functions (A4) and stresses (A5), we need only to carry out the 2D transform on the regular complementary part by standard numerical integration methods, since the full-space solution is available. Because there are no explicit expressions for the complementary part of the solution, we adopt the novel approach proposed by Yang and Pan [18]. The basic idea is as follows. We separate the complementary solution. A known bimaterial solution (two infinite bonded half-spaces), which reflects the mismatch effects of the adjacent upper and lower interfaces in each layer, is subtracted out. Explicit solutions can be obtained for these special terms, and involve only line integrals. Since the bimaterial solution captures the main character of the interface, the remaining complementary part is more smooth and regular. It can be easily obtained with fewer integration quadrature points.

References

[1] B. Clemens, H. Kung and S. Barnett, MRS Bull. 24 **2** 20 (1999).
[2] S. Rao and P. Hazzledine, Phil. Mag. A **80** 2011 (2000).
[3] P. Anderson and Z. Li, Mater. Sci. Engng A **319–321** 182 (2001).
[4] L.P. Kubin, G. Canova, M. Condat, *et al.*, Diffusion Defect Data—Solid St. Data, Part B (Solid St. Phenomena) **23/24** 455 (1992).
[5] K. Schwarz, J. appl. Phys. **85** 108 (1999).
[6] R.M. Zbib, M. Rhee and J.P. Hirth, J. Mech. Sci. **40** 113 (1998).
[7] N.M. Ghoniem, S.-H. Tong and L.Z. Sun, Phys. Rev. **61** 913 (2000).
[8] D. Weygand, L. Friedman, E. Van der Giessen, *et al.*, Modeling Simul. Mater. Sci. Engng. **10** 437 (2002).
[9] R. Martinez and N. Ghoniem, J. Comp. Meth. Engng Sci. CMES **3** 229 (2002).
[10] T. Khraishi, H. Zbib and T. de la Rubia, Mater. Sci. Engng A **309/310** 283 (2001).
[11] J. Lothe, V. Indenbom and V. Chamrov, Phys. Stat. sol. (b) **11** 671 (1982).
[12] B. Von Blanckenhagen, P. Gumbsch and E. Arzt, Modeling Simul. Mater. Sci. Engng. **9** 157 (2001).
[13] T. Gosling and J. Willis, J. Mech. Phys. Solids **42** 1199 (1994).
[14] M. Fivel, T. Gosling and G. Canova, Modeling Simul. Mater. Sci. Engng. **4** 581 (1996).
[15] M. Verdier, M. Fivel and I. Groma, Modeling Simul. Mater. Sci. Engng. **6** 755 (1998).
[16] Y.U. Wang, Y.M. Jin and A.G. Khachaturyan, Acta mater. **51** 4209 (2003).
[17] S. Groh, B. Devincre, L. Kubin, *et al.*, Phil. Mag. Lett. **83** 303 (2003).
[18] B. Yang and E. Pan, Engng Anal. Boundary Element **26** 355 (2002).
[19] B. Yang and E. Pan, Int. J. Solids Struct. **39** 2235 (2002).
[20] S. Rao, C.S.J. Hernandez, T. Parthasarathy, *et al.*, Phil. Mag. A **77** 231 (1998).
[21] N. Ghoniem, S. Tong, J. Huang, *et al.*, J. nucl. Mater. **307** 843 (2002).
[22] D. Barnett and J. Lothe, Physica Norvegica **8** 13 (1975).
[23] T. Ting, *Anisotropic Elasticity: Theory and Applications* (Oxford University Press, New York, 1996).
[24] E. Pan and F. Yuan, Int. J. Solids Struct. **37** 5329 (1999).
[25] F. Yuan, S. Yang and B. Yang, Int. J. Solids Struct. **40** 331 (2003).
[26] T. Mura, in *Advances in Materials Research*, vol. 3, edited by H. Herman (Interscience, New York, 1968), pp. 1–108.
[27] E. Pan, Appl. Math. Modelling **21** 509 (1997).
[28] F. Kroupa, in *Theory of Crystal Defects. Proceedings of the Summer School, Hrazany, September 1964*, edited by B. Gruber (Academia Publishing House of the Czechoslovak Academy of Sciences, Prague, 1966), pp. 275–316.
[29] X. Han, N. Ghoniem and Z. Wang, Phil. Mag. **83** 3705 (2003).
[30] J. Hirth and J. Lothe, *Theory of Dislocations*, 2nd edition (Wiley, New York, 1982).
[31] S. Gavazza and D. Barnett, J. Mech. Phys. Solids **24** 171 (1976).
[32] J. Koehler, Phil. Mag. **2** 547 (1970).